Apatite fission track analysis in the Argentera massif: evidence of contrasting denudation rates in the External Crystalline Massifs of the Western Alps

Serge Bogdanoff[1], André Michard[1,2]*, Mehdi Mansour[3] and Gérard Poupeau[4]

[1]*Laboratoire de Géologie structurale, Université de Paris-Sud, Bâtiment 504, 91405 Orsay, France,*[2]*Laboratoire de Géologie, Ecole Normale Supérieure, 24 rue Lhomond, 75231 Paris cedex 05, France,* [3]*Département de Géologie, Faculté des Sciences Aïn Chock, B.P. 5366, Maarif, Casablanca, Morocco,* [4]*UPRESA 5025 CNRS, Maison des Géosciences, B.P. 53, 38041 Grenoble cedex 9, France*

ABSTRACT

Apatite fission track dating from a central transect in the Argentera massif (southernmost External Crystalline Massif = ECM) yielded ages between 8.05 ± 0.6 and 2.4 ± 0.2 Myr, with a positive age/altitude correlation above 3 Ma, 1200 m. Recognising a thermal peak at *c.* 250°C, 33 Ma, based on stratigraphic, metamorphic and $^{39}Ar/^{40}Ar$ data, the present results suggest a slow cooling rate (8–5°C) for the Argentera massif during the Oligocene–early Pliocene. This rate compares with that from the Pelvoux massif, but contrasts with those observed in the northern ECM (Mont-Blanc and Aar: up to 14°C Myr^{-1}) for the same time interval. This can be related to the different location of the ECM within the collided European margin. At about 3–4 Ma, the denudation rate would have increased up to *c.* 1 mm yr^{-1} in the Argentera massif, reaching the same value as in the Belledonne and northern ECM, likely a consequence of Penninic thrust inversion.

Terra Nova, 12, 117–125, 2000

Introduction

The pre-Triassic basement of the external Western Alps (Helvetic–Dauphinois zone) forms elongated crystalline uplifts at the front of the Penninic–Austroalpine orogenic wedge (Fig. 1). These uplifts, referred to as the External Crystalline Massifs (ECM), form two groups in map view (i) a northern branch including the Aar-Gotthard, Mont Blanc–Aiguilles Rouges, and Belledonne massifs, i.e. an almost continuous, NE-trending line of strongly elevated ECM; and (ii) a southern, more discontinuous branch, including the Pelvoux and Argentera–Mercantour massifs. Recent programmes of deep seismic reflection and refraction profiling have decisively increased our knowledge of the deep structure of the northern ECM (Roure *et al.*, 1990; Blundell *et al.*, 1992; Pfiffner *et al.*, 1997). These massifs correspond to thickened European upper crust (up to 35 km-thick, instead of 20 in the foreland regions) overlying the southeastward plunging European lower crust (Moho at 40–45 km depth). In contrast, the deep structure of the southern massifs is still conjectural, and the Moho depth itself is constrained by relatively scarce seismic informations in the southwestern Alps area (Kissling, 1993; Waldhauser *et al.*, 1998).

*Correspondence:
E-mail: michard@geologie.ens.fr

Up to the present, ECM denudation history has been studied more thoroughly in the northern massifs than in the southern ones. The stratigraphy and subsidence history of the flexural Swiss molasse basin were used by Mugnier and Ménard (1986) to suggest that crustal thickening (stacking of crustal slivers over a basal thrust) of the northern ECM was initiated during the early Miocene. Cooling and denudation histories were derived from zircon and/or apatite fission track data for the Aar and Mont Blanc massifs by Soom (1990), Michalski and Soom (1990), and Seward and Mancktelow (1994), and for the Belledonne massif by Lelarge (1993) and Sabil (1995). Preliminary FT data are also available for the Pelvoux massif (Seward *et al.*, 1999). In the present paper, we focus first on the southernmost ECM, i.e. the Argentera–Mercantour massif, based on the published, geological and isotopic ($^{39}Ar/^{40}Ar$) data, and on apatite fission track (AFT) data thus far only available only in an unpublished doctoral dissertation (Mansour, 1991) and in a preliminary paper by Bigot-Cormier *et al.* 2000). Then, we address the interpretation of the striking differences, which appear in the Oligocene–Miocene cooling rates of the northern and southern ECM, and the possibility of an acceleration in denudation (and uplift?) rate(s) in the southern ECM during the Pliocene.

Geological outline of the Argentera massif

The Argentera–Mercantour massif (Fig. 2) consists of Variscan high-grade schists, migmatites and granites (Bogdanoff *et al.*, 1991; with ref. therein). Tight synclines of Stephanian conglomerates derived from late Variscan grabens were pinched into the Valetta mylonitic zone during early Permian compressional events. Unconformable Permian red beds are found only at the southern border of the massif. Early Triassic sandstones unconformably overlie the older rocks, either around or within the massif (e.g. La Blache, Sespoul, Tortissa synclines), while the remaining of the Mesozoic–Cenozoic cover was detached along the lower Muschelkalk and Keuper evaporitic formations. All around the massif, the Mesozoic cover sheet consists of epicontinental sediments, *c.* 2500 m thick. After a temporary emersion during the Palaeocene–early Eocene (Sturani, 1962; Friès, 1999), marine sedimentation started again with the 1500 m-thick, late Eocene–early Oligocene 'Grès d'Annot' flysch. The latter sequence accumulated in response to flexural bending of the European crust at the front of the advancing Penninic wedge, and ended with the emplacement of the Embrunais–Ubaye and Maritimes Alps flysch nappes (Kerckhove, 1969; Ravenne *et al.*, 1987; Vially, 1994; Lickorish and Ford, 1998). The nappe emplacement was re-

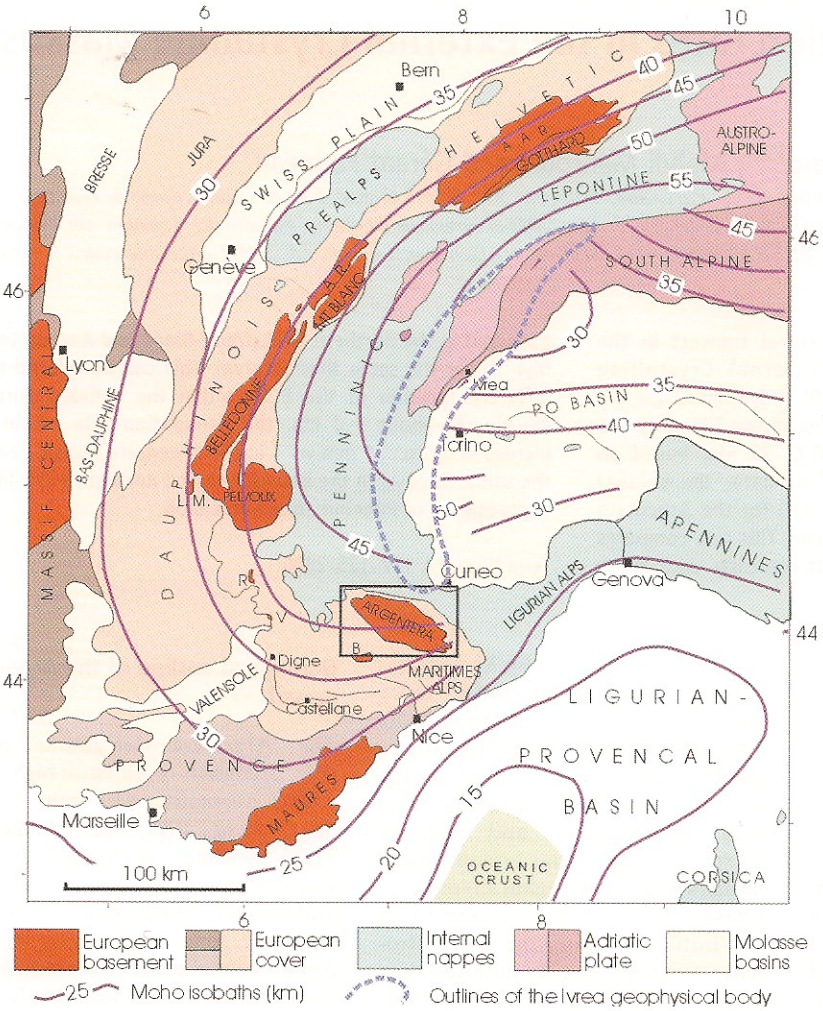

Fig. 1 Geological sketch map of Western Alps and adjacent regions, with location of the study area (framed). Abbreviations: A.R., Aiguilles Rouges; B, Barrot dome; L.M., La Mure; R, Remollon; V, Verdaches. Geological background after the geological map of France, scale 1/1,000,000, 6th edn (1996). Depth of Moho inland after Waldhauser *et al.* (1998). Ligurian-Provençal basin after Chamot-Rooke *et al.* (1997), and Mauffret *et al.* (1995). Ivrea geophysical body after Schmid and Kissling (2000).

sponsible for the early detachment of the Mesozoic–Cenozoic cover sheet (Digne sheet), initiated during the early middle Oligocene as shown by synsedimentary unconformities within the frontal molasse basins (Lemoine, 1972; Ritz, 1992; Lickorish and Ford, 1998).

Within the massif, SW-verging reverse faults, frequently trending parallel to the late Variscan mylonite zones, are evidenced by synclines of Triassic rocks deeply pinched between the footwall and hanging wall blocks (e.g. Sespoul and Tortissa synclines; Bogdanoff, 1986). At the southern front of the massif, basement units are thrust locally over the Permian red beds which deformed into tight reclined folds with N-to NE-dipping axial plane cleavage in low-grade metamorphic conditions (Siddans, 1980; Guardia and Ivaldi, 1985). During the late Miocene–Pliocene, the compressive axis direction turned from SW to N in the Maritimes Alps (Campredon *et al.*, 1977; Labaume *et al.*, 1989; Ritz, 1992), and strike-slip movement occurred on the SW-trending faults (e.g. Bersezio fault; Horrenberger *et al.*, 1978; Labaume *et al.*, 1989). Active tectonics in the Maritimes Alps is still characterized by dominantly N–S to NE–SW compressional stress axes (e.g. Maddedu *et al.*, 1996).

When the cross-section of central Argentera is tentatively represented at crustal scale (Fig. 3), most faults dip steeply close to the surface, particularly in the inner (north-east) part of the massif where back-thrust structures are observed (Fry, 1989). Compared with the northern ECM (Ménard, 1988; Guellec *et al.*, 1990; Hitz and Pfiffner, 1994), it is suggested here that the fault dip progressively decreases at depth below the Argentera, such that the faults would branch into a major shear zone at the top of the lower crust. In our interpretation, the deepest part of the Argentera upper crust is shifted to the NE relative to the topographic crest, consistent with the crustal model calculated by Calais *et al.* (1993) from geodetic data.

Argentera cooling and denudation history

From partial resetting of the $^{39}Ar/^{40}Ar$ chronometer in plagioclase from NW Argentera rocks, Monié and Maluski (1983) concluded that temperature in these rocks reached 220–250°C between *c.* 40 and 33 Ma. We retain an age close to 33 Myr for the temperature maximum, because the burial of the Argentera basement was at a maximum during the earliest Oligocene. Assuming a 25°C km^{-1} mean superficial geotherm (cf. Soom, 1990), and a burial of 9–10 km (summing 4–5 km of autochthonous–parautochthonous cover, and at least 5 km of Penninic nappes), the Argentera rocks would have been at least at 225–250°C at about 33 Ma. More precisely, the studied rocks of central Argentera (sampled at some depth beneath the former basement top) were heated at $250°C < T < 300°C$ as their zircon grains were resetted for FT dating (yielding ages between 29 and 20 Myr: Bigot-Cormier *et al.* 2000), while their biotites were not for K/Ar (yielding Variscan ages; see Hunziker *et al.*, 1992).

Apatite fission track analysis from central Argentera allows us to constrain the latest stages of cooling of the massif below $\pm$ 100°C (e.g. Hunziker *et al.*, 1992). Sixteen samples were collected from the NE-trending transect Isola–Pratolongo, and one additional sample (F3) from western Argentera (Figs 2, 4). After separation, the apatite grains were dated by the population method, using zeta calibration (Table 1, footnote). The ages vary from 8.05 ± 0.6–2.4 ± 0.2 Myr, with the older samples from

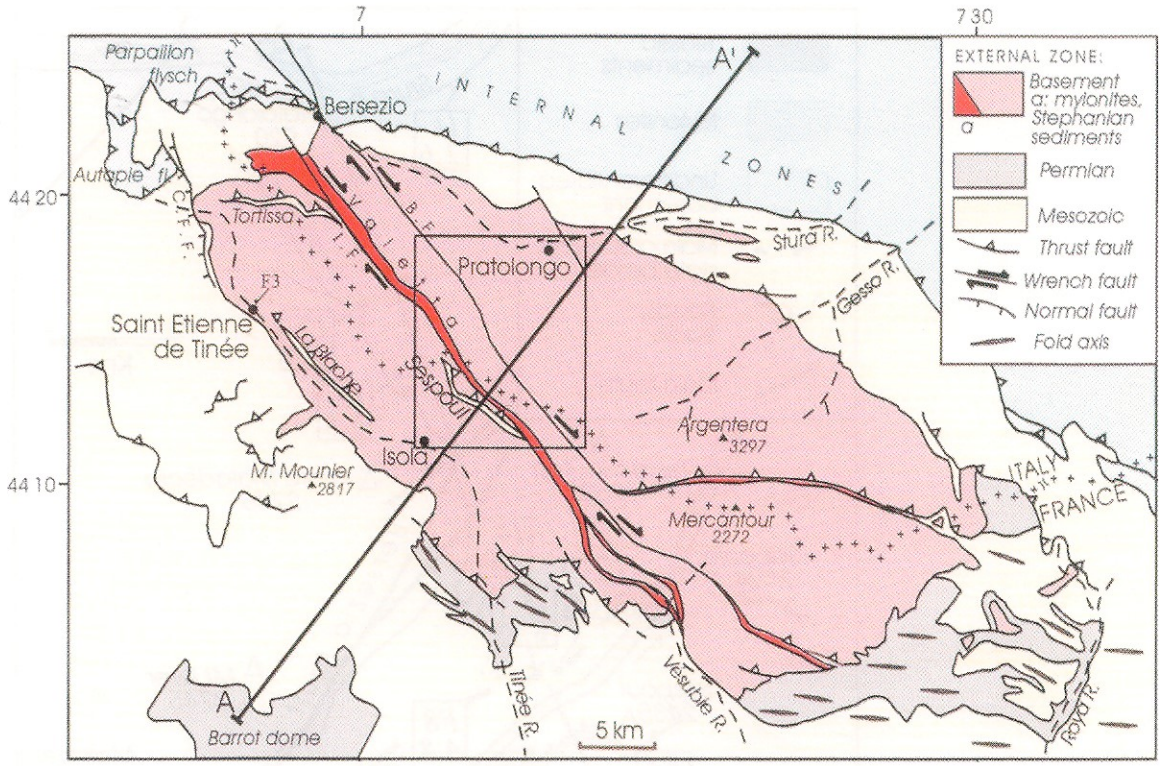

Fig. 2 Geological setting of the Argentera massif, after the geological map of France, scale 1/250,000, sheet 'Gap', and pers. obs. (S. B). AA', cross-section Fig. 3. Framed, sampled area shown in Fig. 4(a); the additional sample F3 (cf. Table 1) is shown close to Saint Etienne de Tinée. Abbreviations: B.F., Bersezio fault; C.F.F., Camp des Fourches fault; I.F., Inciano fault.

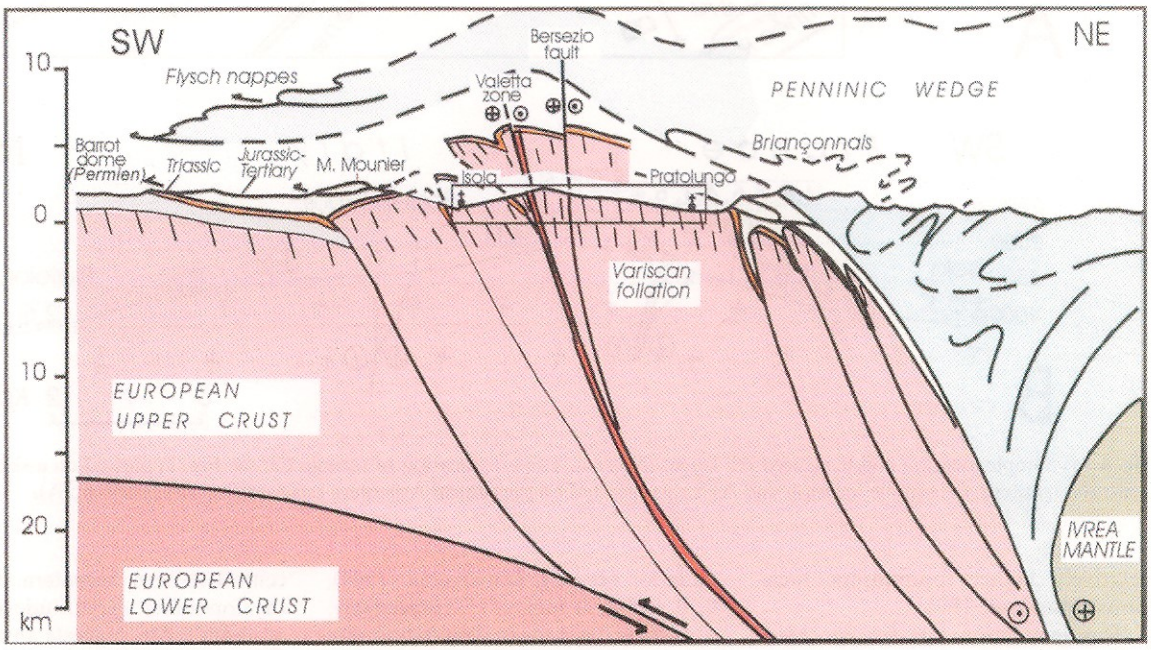

Fig. 3 Generalized cross-section of the Argentera massif (location Fig. 2). Framed, sampled area and cross-section shown in Fig. 4. The interpretation at depth is speculative (see text). Sinistral shear between the Ivrea mantle backstop and the European basement after Ricou and Siddans (1986), and Schmid and Kissling (2000).

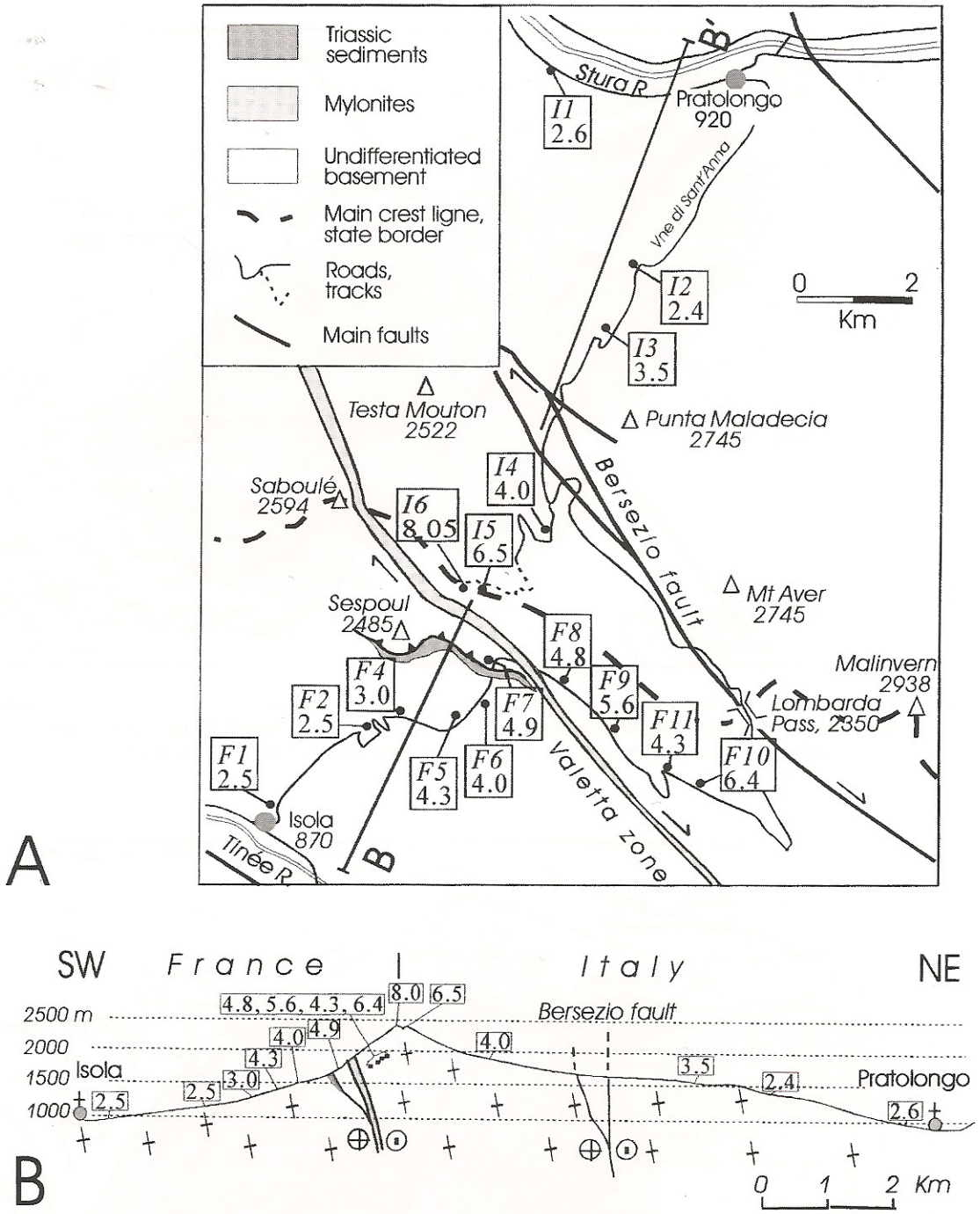

Fig. 4 (a) Sample location and measured AFT ages (Myr; cf. Table 1; location of sample F3: see Fig. 2) plotted on a sketch map of central Argentera. (b) sample location and AFT ages plotted on the central Argentera cross-section (trace BB′ on A).

relatively higher topographic locations (Mansour, 1991).

The denudation rate for late Miocene–Pliocene time can be deduced from the age/altitude diagram (Fig. 5). Between *c.* 8 Ma and 3 Ma, the basement samples lie between two lines which give bounding limits for the denudation rate (e.g. Brown *et al.*, 1994), 0.20 and 0.34 mm yr^{-1}, respectively. This indicates a mean denudation rate close to 0.25 mm yr^{-1} in a moderately differentiated area. A closely similar age/altitude correlation (0.2 mm yr^{-1}) is obtained from independant AFT data by Bigot-Cormier *et al.* (2000) in central–eastern Argentera. A break in the slope of the age/altitude plot (Fig. 5) at about 3 Ma suggests an increase of the exhumation rate up to 0.8–1.5 mm yr^{-1} (dashed lines), with a mean rate of *c.* 1 mm yr^{-1}, nicely consistent with the results obtained by Bigot-Cormier *et al.* (2000) in central and eastern Argentera.

Table 1 Apatite fission track analytical data and ages

Sample	m	n_f (N_f)	$\rho_f \pm 1\ \sigma$ (10^4 t cm^{-2})	n_i (N_i)	$\rho_i \pm 1\ \sigma$ (10^4 t cm^{-2})	N_d	ρ_d (10^5 t cm^{-2})	$t \pm 1\ \sigma$ (Myr)
F1	900	320 (233)	2.21 ± 0.16	80	148.7 ± 4.8	48886 (1416)	5.356 ± 0.024	2.5 ± 0.2
F2	1200	110 (190)	1.60 ± 0.19	110	104.0 ± 3.3	22967 (3098)	5.304 ± 0.035	2.5 ± 0.3
F3	1200	170 (277)	1.45 ± 0.12	99	76.0 ± 2.6	33444 (2487)	4.531 ± 0.025	2.7 ± 0.2
F4	1320	130 (165)	1.92 ± 0.17	80	92.3 ± 6.2	33444 (2442)	4.531 ± 0.025	3.0 ± 0.3
F5	1450	180 (238)	2.00 ± 0.17	90	66.2 ± 3.5	33444 (1969)	4.531 ± 0.025	4.3 ± 0.4
F6	1500	200 (844)	3.90 ± 0.25	200	163.3 ± 5.2	22967 (1413)	5.304 ± 0.035	4.0 ± 0.3
F7	1650	160 (412)	1.95 ± 0.18	150	67.1 ± 2.5	48886 (3331)	5.356 ± 0.024	4.9 ± 0.5
F8	1700	167 (252)	2.28 ± 0.19	130	66.9 ± 3.4	33444 (2759)	4.531 ± 0.025	4.8 ± 0.5
F9	1760	660 (384)	1.75 ± 0.10	165	26.0 ± 1.00	25599 (1416)	2.634 ± 0.016	5.6 ± 0.4
F10	1900	190 (238)	3.23 ± 0.25	65	84.9 ± 6.3	48886 (1824)	5.356 ± 0.024	6.4 ± 0.7
F11	1830	200 (137)	2.51 ± 0.28	80	83.6 ± 6.3	33444 (2212)	4.531 ± 0.025	4.3 ± 0.6
I1	990	200 (237)	3.58 ± 0.24	100	193.2 ± 6.1	33444 (2300)	4.531 ± 0.025	2.6 ± 0.2
I2	1400	170 (223)	0.96 ± 0.07	120	67.0 ± 1.9	48886 (2659)	5.356 ± 0.024	2.4 ± 0.2
I3	1570	200 (115)	2.12 ± 0.23	55	50.6 ± 3.5	25599 (752)	2.634 ± 0.016	3.5 ± 0.5
I4	1900	190 (442)	2.10 ± 0.14	100	87.5 ± 5.2	22967 (2362)	5.304 ± 0.035	4.0 ± 0.4
I5	2400	160 (559)	2.89 ± 0.12	100	76.2 ± 3.3	48886 (2550)	5.356 ± 0.024	6.4 ± 0.4
		143 (463)	2.99 ± 0.31	55	67.6 ± 4.7	48886 (1005)	5.356 ± 0.024	7.4 ± 1.0
								6.5 ± 0.4
I6	2400	180 (174)	0.89 ± 0.08	120	18.0 ± 1.2	22967 (2336)	5.304 ± 0.035	8.2 ± 0.9
		165 (124)	0.70 ± 0.06	60	14.7 ± 1.1	22967 (956)	5.304 ± 0.035	7.9 ± 0.9*
								8.05 ± 0.6

m, altitude, in meters; n_f, n_i, N_f, N_i, numbers of apatite grains (n) and number of tracks counted (N), with suffixes f and i for fossil and induced tracks, respectively; N_d, number of tracks counted in muscovite micas associated to glass dosimeters NBS 962. Errors on track densities were calculated following McGee *et al.* (1985). Sample I5 was counted twice by the same observer (M. Mansour) and sample I6 by two observers (weighted means shown in bold characters). Ages were calculated using zeta values of, respectively, 314 ± 5.4 and for the one with an * of 313 ± 20.

However, the dispersion of the ages of the low-elevation samples could be at least partly a consequence of lateral cooling effect of topographic relief (Stüwe *et al.*, 1994; Mancktelow and Grasemann, 1997). If we apply to the quoted apparent rates the correction suggested by Stüwe *et al.* (1994), the real denudation range of central Argentera in the last 3.5–4 Ma would be close to 0.8–1.0 mm yr^{-1}. Remarkably, during the same time interval, the massif elevation increased by about 1 km (Fauquette *et al.*, 1999).

The earliest cooling stages of the Argentera massif through erosional denudation may be reasonably dated from the early Oligocene, since pebbles from the Penninic nappes (which formed the upper levels of the lid overlying the Argentera–Pelvoux basement at that time) are abundant in the Sannoisian (Rupelian) conglomerates of the Barrême syncline (Graciansky, 1972; Evans and Mange-Rajetzky, 1991), at about 31 Ma (Artoni and Meckel, 1998). Erosional denudation went on during the late Oligocene–Miocene, affecting the Dauphinois cover (cf. pebbles in the Lower–Middle Miocene molasses of the Valensole basin; Haccard *et al.*, 1989), and finally the Permian and basement rocks in the late Miocene (pebbles in the Roquebrune conglomerates close to Nice; Iaworsky and Curti, 1960). Tectonic denudation likely played an increasing role in the denudation process from late Miocene onward (see below). For the 33–8 Ma interval, corresponding approximatively to cooling of the Argentera rocks from 250°C < T > 300°C to

T = 100°C, we may calculate a mean cooling rate of 7–8°C Myr^{-1} (Fig. 6, bold curve). This relatively slow cooling rate is similar to that deduced from the AFT age/altitude diagram (Fig. 5) for the 8–3 Ma interval, assuming a 25°C km^{-1} geotherm (6°C Myr^{-1}). Both rates contrast with the post 3 Ma cooling rate calculated from the same diagram (25–35°C Myr^{-1}).

Discussion and conclusions

Cooling and denudation rates

The juxtaposition of the various ECM cooling paths (Fig. 6) shows that the northern massifs followed much steeper paths than the southern ones during Oligocene–Miocene times. Indeed, burial depth was much greater in the north than in the south. Temperature remained in the 220–250°C range in the Argentera and Pelvoux massifs, but reached 350°C in the Mont Blanc and Aar massifs (e.g. Desmons *et al.*, 1999). This longitudinal thermal gradient is strikingly visible on the K/Ar and Rb/Sr age compilation maps by Hunziker *et al.* (1992), with Variscan or partially reset biotite ages in the Argentera, Pelvoux, southern Belledonne and Aiguilles Rouges massifs, and Eocene–Oligocene biotite ages in the Mont Blanc and Aar massifs. The change in burial depth is related to the change in thickness of the tectonic overload (Penninic wedge), as demonstrated by the concomitant change in the metamorphic grade of the Dauphinois–Helvetic flysch formations, from diagenesis in the Argentera area to anchizone/low-grade metamorphism in internal Pelvoux and Belledonne areas (Leikine *et al.*, 1983; Tricart, 1984; Desmons *et al.*, 1999), to epidote–greenschist facies north-west of Mont Blanc, and, finally, to chloritoid-bearing greenschist facies around the Aar massif (Desmons *et al.*, 1999). Hence, the Penninic wedge overload varied from 3 to 5 km in the Argentera area, to 4–8 km in the Pelvoux and south Belledonne, to 10–14 km in the Mont Blanc and Aar, and the maximum burial depth varied from 8 to 10 km for the southern ECM, to 12–16 km for the northernmost ones. On the other hand, denudation of the ECM was roughly contemporaneous all along the Western Alps, as shown by the sedimentary record in the peri-Alpine molasses. Denudation started during the Oligocene (erosion of the Penninic overload), and was achieved during the Miocene (erosion of the Dauphinois–Helvetic cover, then of the crystalline basement itself), such as pebbles originating from the ECM appear elsewhere in the late Miocene molasses (Trümpy, 1980; Mugnier and Ménard, 1986). Accordingly, the mean denudation and cooling rates between *c.* 30 and 10 Ma had to be much greater in the northern ECM than in the southern ones. Using a 25°C km^{-1} geotherm, the mean cooling rates reported for the Oligocene–Miocene, i.e. for the high temperature range (Fig. 6), correspond to denudation rates of 0.2–0.3 mm yr^{-1} for the southern ECM, and 0.5–0.6 mm yr^{-1} for the northern ECM.

In the low temperature range, AFT age–elevation diagrams from the Belledonne and Argentera massifs would

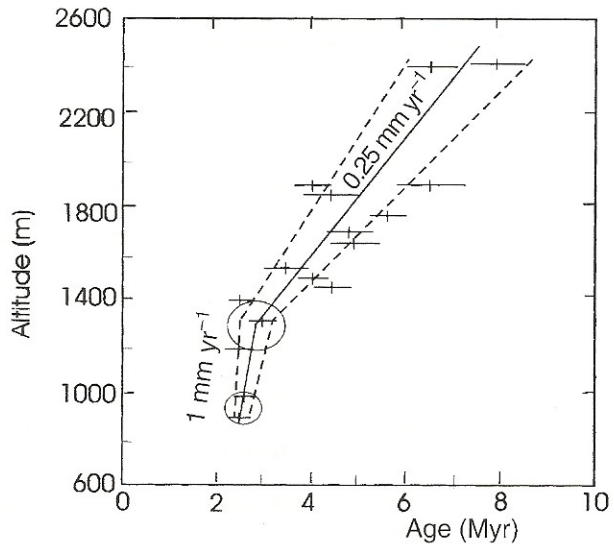

Fig. 5 Apatite fission-track age/altitude correlation diagram for the central Argentera transect (after Mansour, 1991). Error bars 1 σ (cf. Table 1). Sample F3 from the high Tinée valley not plotted.

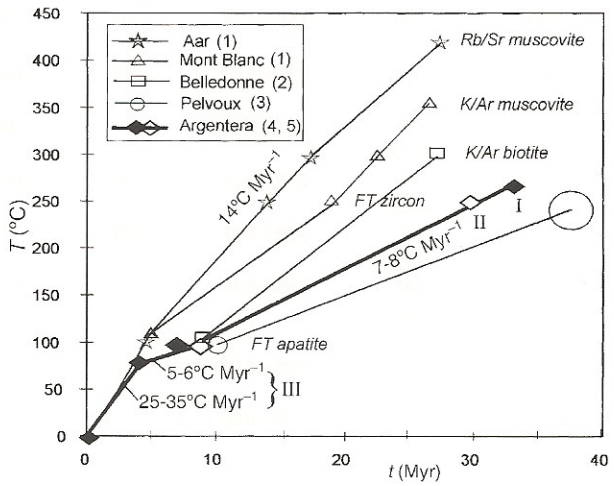

Fig. 6 ECM thermal evolution since the Eocene–Oligocene. Mean cooling paths from the following sources: 1, Soom (1990), and Michalski and Soom (1990); 2, Lelarge (1993); 3, Seward *et al.* (1999); 4, this study; 5, Bigot-Cormier *et al.* (2000). Approximate closure temperature for the different systems (symbols, except I and III) shown after Hunziker *et al.* (1992). I, T–t estimate based on stratigraphy and metamorphism (see text); II, maximum ZFT age from central Argentera (ref. 5); III, cooling curve deduced from AFT data (this study, Fig. 5).

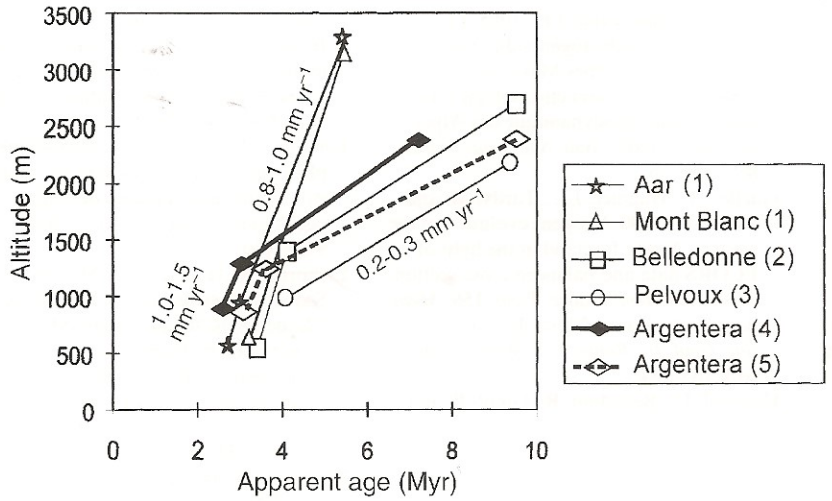

Fig. 7 Comparison of the AFT age/altitude correlation diagrams for the different ECM, with indication of the corresponding denudation rates. Sources: 1, Soom (1990), and Michalski and Soom (1990); 2, Lelarge (1993); 3, Seward *et al.* (1999); 4, this study; 5, Bigot-Cormier *et al.* (2000). Symxbols refer to mean values of key points for each curves.

suggest an increase of the denudation rate at 3–4 Ma (Fig. 7). Some track length optimization runs (Gallagher, 1995) for Belledonne samples also yielded evidence of cooling acceleration at about 2–3 Ma (Sabil, 1995). From that time up to the Present, the denudation rate would have reached 1.0–1.5 mm yr^{-1} in Argentera and Belledonne as in the northern ECM. This apparent rate is overestimated as a result of the effect of eroding topography (Stüwe *et al.*, 1994; Mancktelow and Grasemann, 1997), and would correspond to a real denudation rate of 0.8–1.2 mm yr^{-1} after Stüwe *et al.* (1994) correction. If we accept a broadly steady-state uplift–denudation regime, then a Pliocene denudation rate of *c.*1 mm yr^{-1} would be remarkably consistent with the present-day uplift rate of 0.9–1 mm yr^{-1} observed in the Aar–Mont Blanc (Kahle *et al.*, 1997) and Belledonne massifs (Fourniguet *in* Ménard, 1988).

Tectonic processes

Uplift and exhumation of the northern ECM were driven by compressional stacking of upper crustal slices detached from the internally dipping lower crust, and a similar thickening process is likely in the Argentera (see above). However, shortening of the Alpine realm was more important along the leading (northern) edge of the Adriatic block than along its western boundary (e.g. Schmid *et al.*, 1996). From balanced cross-sections at crustal scale, shortening of the external European upper crust was evaluated at about 30 km and 50 km in the Belledonne and Mont Blanc transects, respectively (Ménard and Thouvenot, 1987; Sommaruga, 1997), while Hitz and Pfiffner (1994) suggest a 25-km shortening for the Aar massif. In the Argentera case, Lickorish and Ford (1998) provide an estimate of *c.* 10 km, based on the structure of the Mesozoic–Cenozoic sheet. Although there are only a few constraints on the individual basement faults, summing their reverse throw along a NE-trending transect (Fig. 3) would rather provide a bulk shortening of about 15 km, which is approximately half of the shortening estimate for the northern ECM. The fact that the Argentera displays about the same crustal thickness (*c.* 40 km, cf. Figure 1) as the northern ECM, in spite of its lesser collisional shortening, may be explained by the greater thickness of the Argentera crust at the end of the Mesozoic rifting, with respect to the typical Dauphinois–Helvetic crust. Indeed, Mesozoic extension of the European margin was less in the Argentera than in the other ECM, as the corresponding, Jurassic–Cretaceous sedimentary facies of the eastern Digne sheet (Maritimes Alps) are thinner and more calcareous than that of the typical Dauphinois domain, more to the west or north-west (Dardeau, 1988; Friès, 1999).

Isostatic uplift of the thickening crust triggered erosion of the sedimentary lid over the Argentera basement during the Oligocene (see above), while tectonic denudation lagged until the Miocene, with the development of SW-dipping normal faults along the SW border of the massif (cf. Camp-des-Fourches fault, Fig. 2; Labaume *et al.*, 1989). Eventually, it can be expected that the post 5 Ma inversion of the Penninic thrusts (Penninic Front, Houiller Front) documented on the Mont-Blanc and Belledonne transects (Seward and Mancktelow, 1994; Fügenschuh *et al.*, 1999) also occurred on the Argentera transect, hence accounting for the high, recent denudation rate (Fig. 7).

Acknowledgements

We thank Gilles Ménard and Stephan Schmid for constructive reviews. Fruitful discussions with Romain Bousquet and Bruno Goffé are also acknowledged.

References

Artoni, A. and Meckel, L.D., 1998. History and deformation rates of a thrust sheet top basin: the Barrême basin, western Alps, SE France. In: *Cenozoic Foreland Basins of Western Europe* (A. Mascle *et al.*, ed.). *Spec. Publ. Geol. Soc. London*, **134**, 213–237.

Bigot-Cormier, F., Poupeau, G. and Sosson, M., 2000. Dénudation différentielle du massif cristallin externe alpin de l'Argentera (Sud-Est de la France) révélées par la thermochronologie traces de fission (apatites, zircons). *C. R. Acad. Sci. Paris*, **330**, 363–370.

Blundell, D., Freeman, R. and Mueller, S. (eds), 1992. *A Continent Revaeled. The European Geotraverse. Geodynamics of Europe*. Cambridge University Press, Cambridge.

Bogdanoff, S., 1986. Evolution de la partie occidentale du massif cristallin externe de l'Argentera. Place dans l'arc alpin. *Géol. France*, **4**, 433–453.

Bogdanoff, S., Ménot, R.P. and Vivier, G., 1991. Les massifs cristallins externes des Alpes occidentales, un fragment de la zone interne varisque. *Sci. Géol. Bull.*, **3–4**, 237–285.

Brown, R.W., Summerfield, M.A. and Gleadow, A.J.W., 1994. Apatite fission track analysis: its potential for the estimation of denudation rates and the assessment of models at long term landscape development. In: *Process Models and Theoretical Geomorphology* (M.J. Kirby, ed.), pp. 25–43. Wiley, Chichester.

Calais, E., Carrier, A. and Buffet, G., 1993. Comparaison des données de nivellement et de positionnement par Global Positioning System: application à la détermination du géoïde dans les Alpes maritimes. *C. R. Acad. Sci. Paris*, **317**, 1493–1500.

Campredon, R., Franco, M., Giannerini, G. *et al.*, 1977. Les déformations des conglomérats pliocènes de l'Arc de Nice (Chaînes subalpines méridionales). *Géol. Méd.*, **4**, 435–438.

Chamot-Rooke, N., Jestin, F. and Gaulier, J.-M., 1997. Constraints on Moho depth and crustal thickness in the Liguro-Provençal basin from a 3D gravity inversion: geodynamic implications. *Rev. Inst. Fr. Pétrole*, **52**, 557–583.

Dardeau, G., 1988. Tethyan evolution and Alpine reactivation of Jurassic extensional structures in the French Alpes maritimes. *Bull. Soc. géol. France*, **4**, 651–657.

Desmons, J., Aprahamian, J., Compagnoni, R., Cortesogno, L. and Frey, M., 1999. Alpine metamorphism of the Western Alps: I. Middle to high T/P metamorphism. *Schweiz. Miner. Petrogr. Mitt.*, **79**, 89–110.

Evans, M.J. and Mange-Rajetzky, M.A., 1991. The provenance of sediments in the Barrême thrust-top basin, Haute-Provence, France. In: *Developments in Sedimentary Provenance Studies* (A.C. Morton *et al.*, eds). *Spec. Publ. Geol. Soc. London*, **57**, 323–342.

Fauquette, S., Clauzon, G., Suc, J.P. and Zhuo Zheng, 1999. A new approach for paleoaltitude estimates based on pollen records: example of the Mercantour Massif (southeastern France) at the earliest Pliocene. *Earth Planet. Sci. Lett.*, **170**, 35–47.

Friès, G., 1999. Evolution de la partie nord-orientale du bassin subalpin de l'Aptien au Nummulitique (SE France). *Bull. Soc. géol. France*, **170**, 531–544.

Fry, N., 1989. Southwestward thrusting and tectonics of the Western Alps. In: *Alpine Tectonics* (M.P. Coward *et al.*, ed.), pp. 83–109. Blackwell Scientific Publications, London.

Fügenschuh, B., Loprieno, A., Ceriani, S. and Schmid, S.M., 1999. Structural analysis of the Subbriançonnais and Valais units in the area of Moûtiers (Savoy, Western Alps): paleogeographic and tectonic consequences. *Int. J. Earth Sci.*, **88**, 201–218.

Gallagher, K.C.J., 1995. Evolving temperature histories from apatite fission track data. *Earth Planet. Sci. Lett.*, **136**, 421–435.

Graciansky, P.C., 1972. Le bassin tertiaire de Barrême (Alpes de Haute Provence): relation entre déformation et sédimentation; chronologie des plissements. *C. R. Acad. Sci. Paris*, **275**, 2825–2828.

Guardia, P. and Ivaldi, J.P., 1985. Les déformations schistogènes du tégument de l'Argentera (Alpes Maritimes): description, genèse et chronologie relative dans le cadre géodynamique des Alpes sud-occidentales. *Bull. Soc. géol. France*, **8**(1), 353–362.

Guellec, S., Mugnier, J.L., Tardy, M. and Roure, F., 1990. Neogene evolution of the western Alpine foreland in the light of ECORS data and balanced cross-section. *Mém. Soc. Géol. France, Paris*, **156**/ *Mém. Soc. Géol. Suisse, Zürich*, **1**/ *Vol. Spec. Soc. Geol. It., Roma*, **1** (F. Roure *et al.*, ed.), 165–184.

Haccard, D., Beaudoin, B., Gigot, P. and Jorda, M., 1989. *Notice explicative, Carte géol. France, feuille La Javie*, scale 1/50 000. Bureau de Recherches Géologiques et Minières, Orléans.

Hitz, L. and Pfiffner, O.A., 1994. A 3D crustal model of the Eastern External Aar Massif interpreted from a network of deep seismic profiles. *Schweiz. Miner. Petrogr. Mitt.*, **74**, 405–420.

Horrenberger, J.C., Michard, A. and Werner, P., 1978. Le couloir de décrochement de Bersezio en Haute-Stura, Alpes externes, (Italie), structure de compression sub-méridienne. *Sci. Géol. Bull.*, **31**, 15–20.

Hunziker, J.C., Desmons, J. and Hurford, A.J., 1992. Thirty-two years of geochronological work in the Central and Western Alps: a review on seven maps. *Mém. Géol. Lausanne*, **13**.

Iaworsky, G. and Curti, M., 1960. La faune des poudingues de Roquebrune (Alpes maritimes). *C. R. Acad. Sci. Paris*, **250**, 399–400.

Kahle, H.G., Geiger, A., Bürki, B. *et al.*, 1997. Recent crustal movements, geoid and density distribution: contribution from integrated satellite and terrestrial measurements. In: *Deep Structure of the Swiss Alps: Results from NRP 20*. (O.A. Pfiffner *et al.*, ed.), pp. 251–259. Birkhaüser, Basel.

Kerckhove, C., 1969. La zone du flysch dans les nappes de l'Embrunais-Ubaye, (Alpes occidentales). *Géol. Alpine*, **45**, 1–204.

Kissling, E., 1993. Deep stucture of the Alps – what do we really know? *Phys. Earth Planet. Int.*, **79**, 87–112.

Labaume, P., Ritz, J.F. and Philip, H., 1989. Failles normales récentes dans les Alpes occidentales: leurs relations avec la tectonique compressive. *C. R. Acad. Sci. Paris*, **308**, 1553–1560.

Leikine, M., Kienast, J.R., Eltchaninoff-Lancelot, C. and Triboulet, S., 1983. Le métamorphisme polyphasé des unités dauphinoises entre Belledonne et Mont Blanc (Alpes occidentales). Relations entre les épisodes de déformation. *Bull. Soc. géol. France*, **4**, 575–587.

Lelarge, L., 1993. Thermochronologie par la méthode des traces de fission d'une marge passive (Dôme de Ponta Grossa, SE Brésil) et au sein d'une chaîne de collision (zone externe de l'Arc alpin, France). Unpubl. doctoral dissertation, Université Joseph Fourier, Grenoble.

Lemoine, M., 1972. Rythme et modalités des plissements superposés dans les chaînes sub-alpines méridionales des Alpes occidentales françaises. *Geol. Rndsch.*, **3**, 975–1010.

Lickorish, W.H. and Ford, M., 1998. Sequential restoration of the external Alpine Digne thrust system, SE France, constrained by kinematic data and synorogenic sediments. In: *Cenozoic Foreland Basins Western Europe* (A. Mascle, *et al.*, eds). *Spec. Publ. Geol. Soc. London*, **134**, 189–211.

Maddedu, B., Béthoux, N. and Stephan, J.F., 1996. Champ de contraintes post-pliocène et déformations récentes dans les Alpes sud-occidentales. *Bull. Soc. géol. France*, **6**, 797–810.

Mancktelow, N.S. and Grasemann, B., 1997. Time-dependent effects of heat advection and topography on cooling histories during erosion. *Tectonophysics*, **270**, 167–195.

Mansour, M., 1991. Thermochronologie par la méthode des traces de fission dans l'apatite. Application aux massifs de l'Argentera-Mercantour (Alpes occidentales) et des Jebilet (Meseta marocaine). Unpubl. doctoral thesis, Université Joseph Fourier, Grenoble.

Mauffret, A., Pascal, G., Maillard, A. and Gorini, C., 1995. Tectonics and deep structure of the north-western Mediterranean basin. *Mar. Petrol. Geol.*, **12**, 645–666.

McGee, V.E., Johnson, N.M. and Naeser, C.W., 1985. Simulated fissioning of uranium and testing of the fission track method. *Nucl. Tracks Radiat. Meas.*, **10**, 365–379.

Ménard, G., 1988. Structure et cinématique d'une chaîne de collision. Les Alpes occidentales et centrales. Unpubl. doctoral thesis, Université Joseph Fourier, Grenoble.

Ménard, G. and Thouvenot, F., 1987. Coupes équilibrées crustales: méthodologie et application aux Alpes occidentales. *Geodinamica Acta*, **1**, 35–45.

Michalski, I. and Soom, M., 1990. The Alpine thermo-tectonic evolution of the Aar and Gotthard massifs, Central Switzerland: fission track ages on zircon and apatite and K/Ar mica ages. *Schweiz. Miner. Petrogr. Mitt.*, **70**, 373–387.

Monié, P. and Maluski, H., 1983. Données chronologiques ^{39}Ar-^{40}Ar sur le socle anté-Permien de l'Argentera-Mercantour (Alpes maritimes, France). *Bull. Soc. géol. France*, **2**, 247–257.

Mugnier, J.L. and Ménard, G., 1986. Le développement du bassin molassique suisse et l'évolution des Alpes externes: un

modèle cinématique. *Bull. c. r. Explor. Prod. Elf Aquitaine*, **10**, 167–180.

Pfiffner, O.A., Lehner, P., Heitzmann, P., Mueller, S. and Steck, A., (eds), 1997 *Deep structure of the Swiss Alps, results from NRP 20*. Birkhaüser, Basel.

Ravenne, C., Vially, R., Riche, P. and Trémolières, P., 1987. Sédimentation et tectonique dans le bassin marin Eocène supérieur-Oligocène des Alpes du Sud. *Rev. Inst. Fr. Pétrole*, **42**, 529–553.

Ricou, L.E. and Siddans, A.W.B., 1986. Collision tectonics in the Western Alps. In: *Collision Tectonics* (M.P. Coward and A.C. Ries, eds). *Spec. Publ. Geol. Soc. London*, **19**, 229–244.

Ritz, J.F., 1992. Tectonique récente et sismotectonique des Alpes du Sud: analyse en termes de contraintes. *Quaternaire*, **3**, 111–124.

Roure, F., Heitzmann, P. and Polino, R. (eds), 1990. Deep structure of the Alps. *Mém. Soc. géol. France, Paris*, **156**/ *Mém. Society géol. suisse, Zürich*, **1**/ *Vol. spec. Soc. geol. It., Roma*, **1**.

Sabil, N., 1995. La datation par traces de fission: aspects méthodologiques et applications thermochronologiques en contexte alpin et de marge continentale. Unpubl. doctoral dissertation, Université Joseph Fourier, Grenoble.

Schmid, S.M. and Kissling, E., 2000. The arc of the western Alps in the light of geophysical data on deep crustal structure. *Tectonics*, **19**, 62–85.

Schmid, S.M., Pfiffner, O.A., Froitzhem, N., Schönborn, G. and Kissling, E., 1996. Geophysical-geological transect and tectonic evolution of the Swiss-Italian Alps. *Tectonics*, **15**, 1036–1064.

Seward, D. and Mancktelow, N.S., 1994. Neogene kinematics of the Central and Western Alps: Evidence from fission track dating. *Geology*, **22**, 803–806.

Seward, D., Ford, M., Burgisser, J., Lickorish, H., Williams, E.A. and Meckel, L.D., 1999. Preliminary results of fission-track analyses in the southern Pelvoux area, SE France. In: *3rd Workshop on Alpine Geological Studies* (G. Gosso *et al.*, ed.). *Mem. Sci. Geol. Padova*, **51**, 25–31.

Siddans, A.W.B., 1980. Compaction, métamorphisme, structurologie des argilites permiennes dans les Alpes maritimes. *Rev. Geol. Dyn. Géogr. Phys.*, **4–5**, 279–292.

Sommaruga, A., 1997. Geology of the central Jura and the Molasse basin: new insight into an evaporite-based foreland fold and thrust belt. *Mém. Soc. Neuchâtel Sci. Nat.*, **12**.

Soom, M.A., 1990. Abkühlungs und Hebungsgeschichte der Externmassive und der penninischen Decken beidseits der Simplon-Rhone-Linie seit dem Oligozän: Spaltspurdatierungen an Apatit/Zircon und K/Ar Datierungen an Biotit/Muscovit (Westliche Zentralalpen). Unpubl. doctoral dissertation, Universität Bern.

Sturani, C., 1962. Il complesso sedimentario autoctono all'estremo Nord-occidentale del Massicio dell'Argentera (Alpi-Marittime). *Mem. Ist. Geol. e Min. Padova*, **23**.

Stüwe, K., White, L. and Brown, R., 1994. The influence of topography on steady-state isotherms. Application to fission track analysis. *Earth Planet. Sci. Lett.*, **124**, 63–74.

Tricart, P., 1984. From passive margin to continental collision: a tectonic scenario for the Western Alps. *Am. Sci.*, **84**, 97–120.

Trümpy, R., 1980. An Outline of the Geology of Switzerlands. In: *Geology of Switzerland; a guide book*. Schweiz. Geol. Komm./ Wepf, Basel.

Vially, R., 1994. The southern French Alps Paleogene basin: subsidence modelling and geodynamic implications. In: *Hydrocarbon and Petroleum Geology of France* (A. Mascle, ed.), *Spec. Publ. Eur. Ass. Petrol. Geosci.* **4**, pp. 281–293. Springer, Berlin.

Waldhauser, F., Kissling, E., Ansorge, J. and Mueller, S., 1998. Three-dimensional interface modelling with two-dimensional seismic data: the Alpine crust–mantle boundary. *Geophys. J. Int.*, **135**, 264–278.

Received 17 August 1999; revised version accepted 26 July 2000.